

Numerical Modeling and Experimental Testing of a Mixed Gas Joule-Thomson Cryocooler

by

John Pettitt

A thesis submitted in partial fulfillment of
the requirements for the degree of

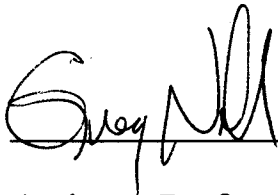
Master of Science
(Mechanical Engineering)

at the

UNIVERSITY OF WISCONSIN-MADISON

2006

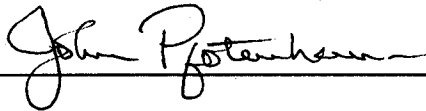
Approved by



Assistant Professor Gregory F. Nellis

4/27/06

Date



Professor John M. Pfothenhauer

4/27/06

Date

Abstract

Mixed gas Joule-Thomson (MGJT) systems have been shown to provide order of magnitude improvements in efficiency relative to JT systems that use pure working fluids. This thesis presents theoretical and experimental work related to using a single-stage, low power (< 1 W) MGJT system for cooling the current leads required by high-temperature superconducting electronics. By thermally integrating the current leads with the recuperative heat exchanger of a MGJT cycle, it is possible to intercept the electrical dissipation and conductive heat leak of the wires at a relatively high temperature which provides a thermodynamic advantage. Also, directly cooling the leads rather than indirectly cooling the chips may provide some advantages relative to thermal integration.

To design the recuperative heat exchanger for the MGJT cycle, the composition of the gas mixture was optimized using a robust genetic optimization technique. Following mixture selection, the optimization model was modified so that it included the effect of frictional pressure drop, axial conduction through the heat exchanger, and the overall conductance available from the heat exchanger on the performance of the MGJT cycle. The individual influences of these loss factors on the refrigeration power of the MGJT cycle were investigated parametrically and conceptually in order to determine the target values for a low power system and develop some insight into the relative importance of each effect. A detailed model of the specific Hampson-style heat exchanger geometry was developed and used to obtain a design for an initial demonstration device.

The demonstration device was fabricated and integrated with a thermal vacuum test facility, gas handling equipment, and the appropriate instrumentation. Several tests were carried out. First, the heat exchanger alone was tested (outside of a JT cycle) using helium as the working fluid. These data provided some experimental verification of the detailed model. Next, the test facility was modified through the installation of a fixed orifice expansion valve to allow open cycle testing of the device using high pressure (9.745 MPa) pure Argon. These measurements provided further insight into the performance of the device.

The test facility was subsequently integrated with a compressor in order to allow measurements of the Device's performance using gas mixtures in a closed loop configuration. These test results ultimately revealed issues relative to contamination, which were addressed through the installation of a liquid nitrogen trap, as well as liquid management. The liquid management issue is thought to be related to inadequate vapor kinetic energy which does not provide sufficient momentum transfer to the liquid to move it through the system. The liquid management issue constrains the performance of the MGJT cycle at low mass flow rates and was explored over a very limited range of conditions. Further testing is suggested which will allow the liquid management constraint to be explored more completely in order to guide future designs.

Acknowledgements

I would like to acknowledge the people who have assisted this project. First, I would like to thank my advisors Greg Nellis and John Pfothauer for giving me their guidance and their patience. They have done an excellent job of creating a positive atmosphere in which to perform this research.

Next, I would like to thank Dan Hoch for sharing his vast expertise and intuition with me; and for sharing his genuine friendship with me. I would also like to thank Sandy Klein for EES and the way it changed my thinking; Natalie Meagher and Steve Meitner, who assisted with several experimental aspects of this project. And finally, I want to acknowledge the Office of Naval Research for their financial support of this research.

Table of Contents

Chapter 1 – Introduction.....	1
1.1 Actively cooled current lead concept.....	1
1.2 Mixed Gas Joule Thomson Cycle.....	4
1.3 Thesis Organization.....	15
Chapter 2 – Numerical Modeling.....	18
2.1 Mixture Selection.....	18
2.1.1 Mixture Properties.....	18
2.1.2 Optimization Model.....	19
2.1.3 Optimization.....	28
2.2 Cycle Performance Model.....	40
2.3 Detailed Model of Heat Exchanger Geometry.....	42
2.3.1 Description of Geometry.....	42
2.3.2 Heat Exchanger Calculation.....	44
2.3.3 Heat transfer Prediction.....	51
2.3.4 Pressure Drop Prediction.....	54
2.3.5 Axial Resistance Calculation.....	56
2.4 Design.....	59
2.4.1 Design Methodology.....	59

2.4.2 Design Constraints.....	62
2.4.3 Device A Design.....	70
2.4.4 Device B Design.....	79
Chapter 3 – Experimental Testing.....	91
3.1 Device A Fabrication.....	91
3.2 Test Facility and Instrumentation.....	94
3.3 Open JT Cycle Argon Testing.....	108
3.4 Closed JT Cycle Testing.....	113
3.4.1 Oct 26 – Nov 28, 2005.....	115
3.4.2 Dec 1, 2005 – Jan 5, 2006.....	121
3.4.3 Jan 10 – March 20, 2006.....	139
3.5 Testing Summary.....	147
Chapter 4 – Summary.....	151
References.....	154
Appendix A.....	156

List of Figures

1.1 The conventional cooling configuration used for high temperature superconducting electronics.....	1
1.2 The proposed method of cooling HTS electronics.....	3
1.3 Component diagram for a Joule-Thomson cycle.....	5
1.4 Maximum cooling power per unit of mass flow rate for a closed JT cycle using argon and nitrogen as a function of hot end temperature for operating pressures of 100 kPa and 1000 kPa.....	7
1.5 Maximum cooling power per unit of mass flow rate for a closed JT cycle as a function of hot end temperature for operating pressures of 100 kPa and 1000kPa.....	8
1.6 Enthalpy difference between 1000 kPa and 100 kPa (i.e., maximum cooling capacity per mass flow rate) as a function of temperature for nitrogen and a mixture of 14% N ₂ /8% CH ₄ /78% C ₂ H ₆ (by mole).....	9
1.7 Pressure-enthalpy diagram for (a) pure nitrogen and (b) a mixture of 14% N ₂ /8% CH ₄ /78% C ₂ H ₆ (by mole).....	10
1.8 Schematic drawing of bellows control self-regulating JT cooler.....	14
2.1 The recuperative heat exchanger broken into N segments of equal recuperative heat transfer.....	20
2.2 Differential energy balance on one heat exchanger segment.....	23
2.3 Saturation temperature of mixture components as a function of pressure.....	30
2.4 Optimal composition and refrigeration power per unit heat exchanger conductance for $\dot{Q}_{load,dist} / \dot{Q}_{load,cold} = 1$	31
2.5 Optimal composition and refrigeration power per unit heat exchanger conductance for $\dot{Q}_{load,dist} / \dot{Q}_{load,cold} = 0$	32
2.6 The refrigeration capacity per unit of conductance associated with receiving half of the total heat load in a distributed fashion is 15%, on average, over a wide range of ΔT	33

2.7 The minimum cycle temperature for the optimal mixtures found for $\dot{Q}_{load,dist} / \dot{Q}_{load,cold} = 0$ and $\dot{Q}_{load,dist} / \dot{Q}_{load,cold} = 1$	34
2.8 The refrigeration power per unit of mass flow rate for the optimal mixtures found for $\dot{Q}_{load,dist} / \dot{Q}_{load,cold} = 0$ and $\dot{Q}_{load,dist} / \dot{Q}_{load,cold} = 1$	34
2.9 Minimum cycle temperature for the “freeze-tolerant” mixture in Table 2.2.....	37
2.10 Refrigeration per unit of heat exchanger conductance for the design mixture and the operating conditions of Table 2.2. The refrigeration per unit mass flow rate (\dot{Q} / \dot{m}) is the same for both modes of receiving the heat load.....	38
2.11 Required heat exchanger conductance per unit mass flow rate as a function of hot end temperature difference.....	39
2.12 Hampson style heat exchanger. The mandrel and shell act only as support structures and pressure barriers; only the helically wound tube (i.e. the finned tube in the figure, although the fins are not shown) provides heat transfer area.....	43
2.13 Cross-sectional view (along the axis) of a Hampson style heat exchanger. The low pressure stream travels through the array of fins presented by the finned tube while the high pressure stream is carried by the tube itself.....	44
2.14 Resistance network for the i^{th} control volume.....	46
2.15 Thermal conductivity as a function of temperature.....	49
2.16 Percent change between the thermal conductivity at 300 K and the thermal conductivity at lower temperatures.....	50
2.17 Transverse (T_p) and Longitudinal pitch (L_p) for Hampson heat exchanger.....	55
2.18 Parallel circuit network for R_{axial} calculation. $T[i-1]$ is warmer than $T[i]$	56
2.19 Performance prediction process.....	59
2.20 Design search method.....	61
2.21 Refrigeration capacity as a function of mass flow rate for $\Delta T = 0K, 3K,$ and $6K$ (with no other losses).....	63
2.22 Heat exchanger conductance required to provide the refrigeration shown for $\Delta T_{hot} = 3K$	64

2.23 Refrigeration power as a function of mass flow rate and the stated conductance. The $\Delta T_{hot} = 0\text{K}$ case requires an infinite conductance.....	65
2.24 Refrigeration power per unit mass flow rate as a function of hot stream pressure drop ($\Delta T = 3\text{K}$).....	67
2.25 The loss in refrigeration power as the inlet pressure to the orifice is lowered by pressure drop through the hot stream.....	68
2.26 The axial conduction loss as a function of the axial conduction thermal resistance at the design conditions.....	69
2.27 Finned tube at 50 X magnification.....	71
2.28 Axial resistance of the selected mandrel/shell/finned tube assembly as a function of heat exchanger length.....	75
2.29 The required conductance for $\Delta T_{hot} = 3\text{ K}$ and the conductance function for Device A.....	76
2.30 Hot stream pressure drop of Device A.....	77
2.31 The influence of the various loss factors on the performance of Device A.....	78
2.32 Multiple finned tubes in parallel (the fins are not shown).....	80
2.33 Refrigeration power of multiple tubes using a 6.35 mm (0.25 in) mandrel (i.e., Design #1).....	85
2.34 Refrigeration power of multiple tubes using a 9.53 mm (0.375 in) mandrel (i.e., Design #2).....	85
2.35 Refrigeration power of multiple tubes using a 12.7 mm (0.5 in) mandrel (i.e., Design #3).....	86
2.36 Maximum finned tube length for the mandrel length of 0.315 m.....	87
2.37 Conductance as a function of mass flow rate for various numbers of tubes and a 12.7 mm (0.5 in) mandrel (Design 3).....	88
2.38 Axial conduction loss as a function of the number of finned tubes for various mandrel diameters.....	89
2.39 Predicted refrigeration as a function of mass flow rate for Device B.....	90
3.1 Design of Device A.....	92

3.2 Test facility schematic.....	94
3.3 Temperature measurement fixture for PRT.....	97
3.4 One end of the tube-in-tube heat exchanger used for the shake-down testing.....	98
3.5 Ineffectiveness based on the cold stream heat transfer rate as a function of the mass flow rate for Device A while operated with pure helium and cooled with liquid nitrogen.....	101
3.6 Difference between measured cold and hot stream heat transfer rate as a function of the mass flow rate for Device A while operated with pure helium and cooled with liquid nitrogen.....	102
3.7 Heat exchanger conductance as predicted by the detailed model and based on the cold stream heat transfer rate from the helium test data.....	103
3.8 Predicted hot stream Reynolds number as a function of the assumed linear temperature profile and mass flow rate for Helium test data.....	104
3.9 Heat exchanger conductance correlation comparison.....	105
3.10 Percentage of the parasitic heat load relative to the cold stream heat transfer.....	106
3.11 Hot stream pressure drop as a function of mass flow rate for Helium test data.....	107
3.12 Facility schematic for open JT cycle experiments with pure argon.....	108
3.13 Cold end heat load as a function of the cold inlet temperature for open cycle argon tests employing 76.2 μm (0.003 in) orifice.....	109
3.14 T-h diagram for argon and the approximate operating conditions of the open cycle.....	111
3.15 Gas handling equipment integrated with test facility.....	114
3.16 Temperature data for 152.4 μm (0.006 in) orifice.....	116
3.17 Temperature data for 101.6 μm (0.004 in) orifice.....	116
3.18 Temperature data for 63.5 μm (0.0025 in) orifice.....	117
3.19 Facility schematic after initial closed cycle testing with design mixture.....	118
3.20 Temperature data for 11-21-05 test run.....	119
3.21 Temperature data for 11-28-05 test run.....	120
3.22 Temperature data for Test run 12-01-05.....	122
3.23 Temperature and flow rate data for Test run 12-07-05.....	124

3.24	Temperature data for test runs 12-01-05 and 12-07-05.....	125
3.25	Liquid Nitrogen Trap.....	127
3.26	Temperature and flow rate data for test run 12-23-05.....	128
3.27	Temperature and flow rate data for test run 12-28-05.....	130
3.28	Component saturation temperature as a function of gauge pressure.....	131
3.29	Temperature and flow rate data for test run 12-30-05.....	132
3.30	Temperature and flow rate data of test run 01-03-06.....	134
3.31	Cold end temperatures for test run 01-03-06.....	135
3.32	Temperature and pressure data for test run 01-03-06.....	136
3.33	Flow reduction event for test 01-03-06.....	136
3.34	P-h diagram for ethane and some test data from test run 01-03-06.....	137
3.35	Temperature and flow rate data for test run 01-05-06.....	139
3.36	Stainless steel liquid nitrogen trap.....	142
3.37	Heat exchanger hot outlet and cold inlet temperature as a function of initial inlet pressure for the test runs in Table 3.21 and Table 3.22.....	144
3.38	Flow rate data comparison of design mixture test runs 02-08-06 and 03-01-06.....	145

List of Tables

1.1 Dimensions of the heat exchanger described by Ng et al. (2000).....	12
2.1 Design conditions.....	29
2.2 Allowable composition variation and new operating conditions for a “freeze-tolerant” mixture.....	36
2.3 Experimental coefficients for thermal conductivity.....	49
2.4 Single-phase heat transfer for the i^{th} segment of the hot stream.....	52
2.5 Single-phase heat transfer for the i^{th} segment of the cold stream.....	53
2.6 Single-phase pressure drop in the hot and cold streams.....	54
2.7 Finned tube dimensions for Device A.....	70
2.8 Inner and outer tube dimensions for Device A.....	73
2.9 Finned tube dimensions for Device B.....	81
2.10 Assumed fabrication limits to multiple tube design.....	82
2.11 Shell and mandrel illustration designs.....	84
2.12 Shell and mandrel for Device B.....	89

List of Variables

A	Area (m ²)
A_b	Surface area of tube base (m ²)
A_f	Area of a fin (m ²)
A_{ff}	Free-flow area (m ²)
cp	specific heat (kJ/kg-K)
D_{helix}	Diameter of helix (m)
err	Percent Error
Fin_{OD}	Fin diameter (m)
$Fins_{inch}$	Fins per inch (1/in)
G	Mass flux (kg/s-m ²)
h	Enthalpy (J/g)
htc	Heat transfer coefficient (W/m ² -K)
ID	Inner Diameter (in or m)
k	Thermal conductivity (W/m-K)
L	Length (m)
L_{fins}	Length or height of fins from tube base (m)
L_p	Longitudinal pitch (m)
\dot{m}	Mass flow rate (g/s or kg/s)
M	Number of heat exchanger segments in detailed model (equal lengths) (-)
N	Number of recuperative heat transfer segments in optimization model (-)
N_{fins}	Number of fins (-)
Nu	Nusselt number (-)
N_T	Number of Tubes (-)
OD	Outer Diameter (in or m)
P	Pressure (kpa or psig)
Pr	Prandtl number
$\dot{Q}_{load,cold}$	Heat load applied to cold end of heat exchanger (W)
$\dot{Q}_{load,dist}$	Distributed heat load along the heat exchanger length (W)
\dot{Q}_{rec}	Recuperated heat (kJ/kg)
\dot{Q}_{rej}	Heat Rejected from cycle to surroundings (J/g)
R	Thermal resistance (K/W)
r	Radius (m)
Re	Reynolds number (-)
r_{ft}	Fin radius on finned tube (m)
Sbc	Spacing between coils (m)
Sbc_{adj}	Spacing between adjacent coils (m)
S_{ft}	Spacing between fins (m)
t	Thickness (m)
T	Temperature (K)
tf_{ft}	thickness of fin on the finned tube (m)

T_p	Transverse pitch (m)
UA	Heat exchanger stream-to-stream conductance (W/K)
\dot{V}	Volume flow rate (L/min or Ft ³ /hr)
\dot{W}_{comp}	Isentropic compressor work (J/g)
X_T	Non-dimensional Transverse pitch (-)
X_L	Non-dimensional Longitudinal pitch (-)
y_i	Mole fraction of component i of mixture

Greek

ΔT	Hot end temperature difference (K)
η	Fin efficiency (-)
η_o	Overall fin efficiency (-)
μ	Dynamic viscosity (kg/m-s)

Subscripts

$h/high/hot/HP$	Associated with the high pressure or hot stream
$c/low/cold/LP$	Associated with the low pressure or cold stream
$inlet$	Entrance to cryostat/experiment
$outlet$	Exit of cryostat/experiment
$freeze$	Freezing temperature
tp	Triple point
sat	Saturation state
$spec$	Specified by geometry
$axial$	Straight line between the hot end and cold end of the heat exchanger
$cond$	Conduction heat transfer in the axial direction
ft	Associated with the finned tube
ot	Outer tube
it	Inner tube
tot	Total or sum

Chapter 1 Introduction

1.1 Actively Cooled Current Leads

High temperature superconducting (HTS) electronics are being developed in order to operate in the temperature range of 80 K to 120 K. These electronic components must be mounted on a cold stage that is actively cooled via a thermal connection with any one of several types of commercially available cryocoolers, as shown in Figure 1.1. A large part of the heat load on the system is related to the current leads that carry the bias current and signals from room temperature electronics. The heat leak from these wires onto the high temperature superconducting chips is related to conduction along the leads as well as ohmic dissipation (because these leads are not superconducting).

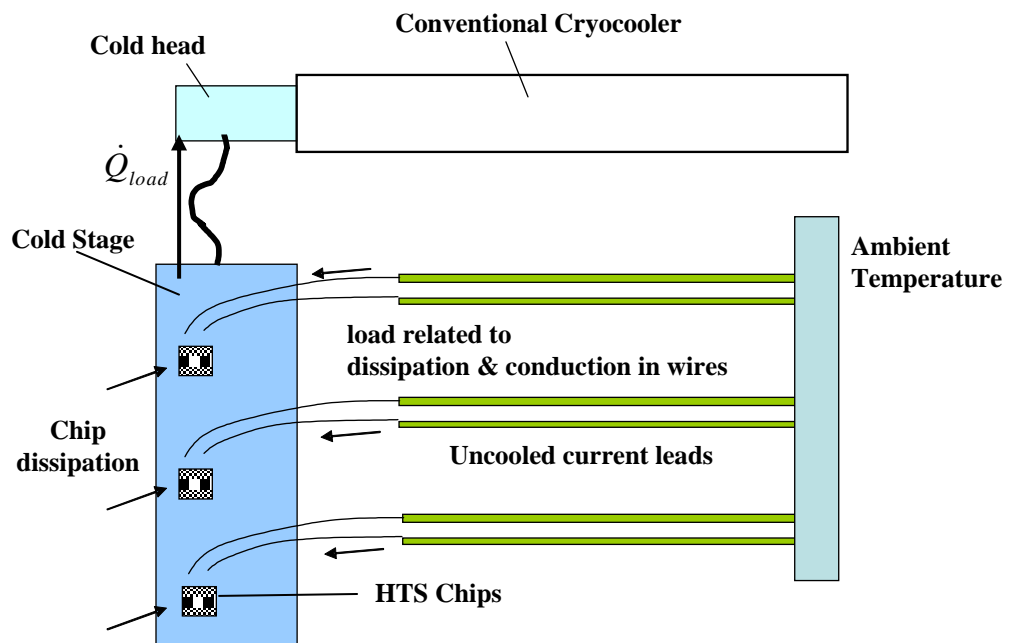


Figure 1.1: The conventional cooling configuration used for high temperature superconducting electronics.

There are two disadvantages associated with the cooling configuration shown in Figure 1.1. Thermal integration with the cryocooler is difficult. The current leads deposit thermal loads throughout the electronics package at the various electrical connections however the cooling load is removed from a single thermal interface with the cold stage. Therefore, chips mounted closer to the cold stage will be colder than those mounted further away. The performance of superconducting electronics is sensitive to temperature and it is important that interfacing chips be at the same temperature.

Also, the heat is allowed to reach the lowest temperature part of the cycle before it is removed. Entropy is the ratio of heat transfer to temperature and therefore, the heat load represents the largest entropy flow at the coldest point in the cycle. The power and size requirements of the cryocooler generally scale with the entropy flow that it must remove and therefore there is a thermodynamic advantage associated with removing the heat load at a higher temperature.

Ideally, the entire electronics package would be kept at a uniform cryogenic temperature and the heat generated by ohmic dissipation would be removed at a temperature very near where it was generated. Several researchers, including Williams (1963), have shown that cooling current leads carrying high currents for large superconducting magnets with vapor cryogen allow for much of the heat leak to be intercepted before it reaches the cold end. Vapor cooling current leads for high temperature superconducting electronics has not previously been studied. The direct implementation of vapor cooling via the boil-off

of a cryogen is not likely to be feasible for applications that require a gravity independent system due to the presence of the liquid.

The objective of this thesis is to study a system in which the current leads are thermally integrated with the recuperative heat exchanger within a mixed gas Joule-Thomson (MGJT) system, as shown in Figure 1.2. The recuperative heat exchanger removes the conductive and ohmic heat leak of the current leads at the temperature where it is generated and also provides cooling to the HTS computer chips at several locations in the electronics package. The cooling is provided via the leads rather than indirectly (as shown in Figure 1.2). This actively cooled current lead concept has thermal integration and thermodynamic advantages; the configuration may permit a more uniform temperature distribution from chip-to-chip and also allow heat to be removed from the system in a more reversible manner.

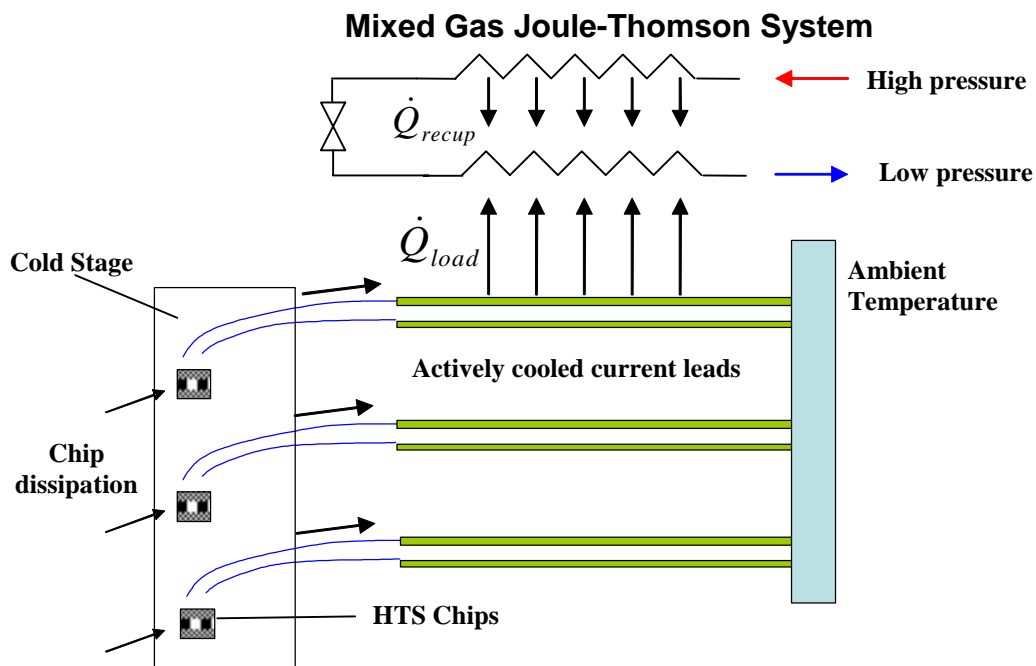


Figure 1.2: The proposed method of cooling HTS electronics.

This project has focused primarily on the details of the MGJT refrigeration cycle; while there has been substantial research in this area, there has been relatively little detailed theoretical work reported that supports the more numerous publications regarding specific experimental results. Also, the use of an MGJT system for high efficiency, low power, low temperature applications involving a distributed load has not been thoroughly studied. In the following sections, JT and MGJT systems are introduced and discussed.

1.2 Mixed Gas Joule-Thomson Cycle

The simplest, closed cycle configuration for a Joule-Thomson system is shown in Figure 1.3. The cycle consists of a compressor, an aftercooler, a recuperative heat exchanger, a valve, and an evaporator or load heat exchanger. In this cycle, the working fluid is compressed to a high pressure (state 2) and cooled to room temperature (state 3) in the aftercooler. The high pressure gas enters the recuperative heat exchanger and is cooled (by the returning low pressure gas) until it exits the heat exchanger at a cryogenic temperature (state 4). The high pressure, cold working fluid is expanded through a valve; this isenthalpic expansion causes the temperature of the fluid to drop (state 5). The cold, low pressure fluid accepts heat as it passes through the load heat exchanger or evaporator. The working fluid enters the cold end of the heat exchanger (state 6) and warms as it pre-cools the high pressure gas until finally it exits the heat exchanger and enters the suction side of the compressor (state 1).

